E-proceedings of the 36th IAHR World Congress
28 June – 3 July, 2015, The Hague, the Netherlands

BROAD-CRESTED WEIR OPERATION UPSTREAM OF A STEEP STEPPED SPILLWAY

GANGFU ZHANG[1], & HUBERT CHANSON[2]

[1] The University of Queensland, School of Civil Engineering, Brisbane QLD 4072, Australia
e-mail: gangfu.zhang@uqconnect.edu.au

[2] The University of Queensland, School of Civil Engineering, Brisbane QLD 4072, Australia
e-mail: h.chanson@uq.edu.au

ABSTRACT

New experiments were performed on a large-size stepped spillway facility. The operation of the broad-crested weir was characterised together with the steep (1V:1H) stepped chute. The introduction of a small rounding at the crest's downstream end was shown to prevent jet deflection. The hydraulics of the weir overflow was examined, and the results showed critical flow conditions (i.e. minimum specific energy) along most portions of the crest, although the pressure distributions were not always hydrostatic and the velocity profiles were not uniform. The stepped chute flow was highly aerated. The two-phase flow in the stepped chute was characterised in details. The air-water flow properties were analysed in terms of the rate of energy dissipation, showing 60% of energy dissipation rate down the first 12 steps..

Keywords: *Broad-crested weir, Steep stepped spillway, Physical modelling, Jet deflection*

1. INTRODUCTION

Dams and reservoirs are man-made hydraulic structures built across rivers and streams to provide water storage. During a major rainfall, the large inflows into the reservoir induce a rise in water level with the risk of dam overtopping. The spillway system is a structure designed to spill safely the flood waters above, below or besides the dam wall. Most small dams are equipped with an overflow structure, the spillway, which includes typically a crest, a chute and an energy dissipator at the downstream end (USBR 1965, Novak et al. 2011). The energy dissipator is designed to dissipate the excess in kinetic energy at the end of the spillway before it re-joins the natural stream. Energy dissipation is typically achieved by a standard stilling basin downstream of a steep spillway chute in which a hydraulic jump takes place, a high velocity water jet taking off from a ski jump and impinging into a downstream plunge pool, or a plunge pool in which the chute flow impinges and the kinetic turbulent energy is dissipated in turbulent recirculation. The construction of steps on the steep spillway chute may assist also with the energy dissipation (Fig. 1). The stepped channel design has been used for more than 3 millenia (Knauss 1995, Chanson 2001). A large number of stepped spillways were built with a stepped spillway systems during the 19th century through to the early 20th century (Wegmann 1906, Schuyler 1909), when the design technique became outdated with the development of hydraulic jump stilling basin designs. Recent advances in construction materials and technology, including roller compacted concrete (RCC) and polymer-coated gabion wire, led to a regain in interest for the stepped chute design (Chanson 1995,2001).

Herein a physical investigation was conducted in laboratory with a focus on the operation of a steep stepped spillway located downstream of a broad-crested weir. New experiments were conducted in a large size facility. The observations included a series of detailed measurements to characterise the broad-crest operation, the introduction of a simple device to prevent jet deflection at the crest's downstream end and thorough air-water flow measurements down the steep stepped chute.

Figure 1. Concrete dam stepped spillways. (Top) Hinze dam (stage 3) stepped spillway (Australia) with the stilling basin in the foreground on 24 October 2014; (Bottom) Riou dam stepped spillway (France) on 11 February 2004

2. EXPERIMENTAL FACILITY AND INSTRUMENTATION

2.1 Experimental facility and instrumentation

New experiments were conducted in a new large-size stepped spillway model located at the University of Queensland. The facility consisted of a 12.4 m long channel. Three pumps driven by adjustable frequency AC motors delivered a controlled discharge to a 5 m wide, 2.7 m wide and 1.7 m deep intake basin, leading to a 2.8 m long side-wall convergent with a contraction ratio of 5.08:1, resulting in a smooth and waveless flow. The inflow upstream of the test section was controlled by a broad-crested weir. The weir was horizontal, 0.6 m long and 0.985 m wide with a vertical upstream wall and an upstream rounded nose (0.058 m radius). During initial tests, the weir ended with a sharp edge. Later a downstream rounded edge (0.018 m radius) was installed and all experiments were conducted with the downstream edge rounding. The crest was made of smooth, painted marine ply and followed by 12 smooth impervious flat steps made of plywood. Each step was 0.1 m long, 0.1 m high and 0.985 m wide. The stepped chute was followed by a horizontal tailrace flume ending with a free overfall.

Above the broad-crested weir, velocity and pressure measurements were performed with a Dwyer® 166 Series Prandtl-Pitot tube connected to an inclined manometer, giving total head and piezometric head data. The tube was made of stainless steel, and featured an hemispherical total pressure tapping (Ø = 1.19 mm) at the tip with four equally spaced static pressure tappings (Ø = 0.51 mm) located 25.4 mm downstream of the tip. The tube design met AMCA and

ASHRAE specifications. The vertical movement of the Prandtl-Pitot tube was controlled by a fine adjustment travelling mechanism connected to a Mitutoyo™ digital scale with an accuracy of ±0.01 mm. The accuracies of the longitudinal and transverse positions of the tube were estimated to be ±0.5 cm and ±1 mm respectively. Clear-water flow depths were measured with a pointer-gauge on the channel centreline as well as dSLR photography (Canon™ 400D) through the sidewalls. Lens distortion was corrected with the software PTLens 8.7.8. The photographic and pointer-gauge depth measurements agreed within ±0.5mm.

The air-water flow measurements were conducted using a dual-tip phase detection probe developed at the University of Queensland. The probe was capable of recording rapidly varying air-water interfaces based upon changes in resistivity and consisted of two identical tips, with an inner diameter of 0.25 mm, separated longitudinally by 7 mm. The probe sensors were excited by an electronic system and the signal output was recorded at 20 kHz per sensor for 45 s, following previous sensitivity analyses (Toombes 2002; Felder and Chanson 2015). A trolley system used to position the probes was fixed by steel rails parallel to the pseudo-bottom between step edges and the probe's vertical movement was controlled by a Mitutoyo™ digital ruler within ±0.01mm.

Figure 2. Skimming flow above the stepped spillway model - Flow conditions: h = 0.1 m, l = 0.1 m, d_c/h = 1.1 - (Top) General view; (Middle) Skimming flow above cavity recirculations, with flow direction from right to left; (Bottom) Looking downstream at the upper spray region and splash structures

3. Flow patterns

3.1 Presentation

The discharge on the steep stepped chute was controlled by the upstream broad crested weir (Fig. 2 Top). Quiescent inflow conditions were observed for all investigated discharges above the broad-crested weir (Fig. 3 Top). The flow

accelerated above the upstream rounded nose. The flow was rapidly varied next to the upstream end of the crest and characterised by some rapid change in free-surface curvature and pressure and velocity distributions (Fig 4 Bottom). For moderate to large discharges (H_1/L_{crest} > 0.17), the free-surface fell continuously along the crest, implying that the flow was accelerated and pressure gradient was not hydrostatic in regions of large streamline curvature. For the smallest discharges (H_1/L_{crest} < 0.11), the water-surface above the crest showed some characteristic wavy shape and the overflow was subcritical. The finding may be linked with the effect of a pseudo-laminar boundary layer at low flow rates which caused some energy loss (Isaacs 1981).

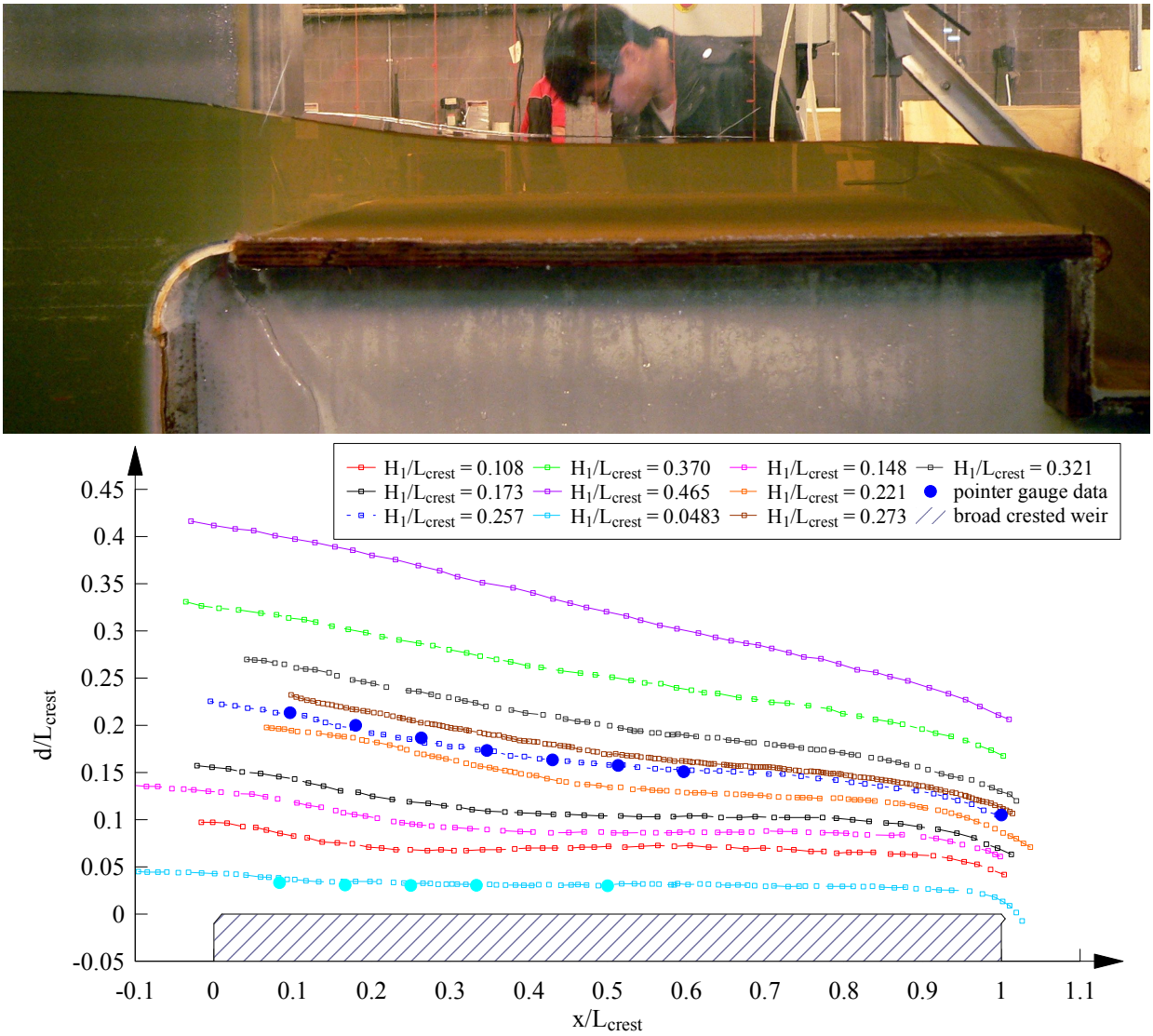

Figure 4. Broad-crested weir overflow. (Top) Side view for H_1/L_{crest} = 0.173; both upstream and downstream roundings are clearly visible; (Bottom) Dimensionless free-surface profiles ; comparison between photographic and pointer gauge (solid circles) data

3.2 Discussion

Initial test were conducted with a sharp downstream crest edge. Un-ventilated deflected jets were observed for 0.15 < H_1/L_{crest} < 0.44, where H_1 is the upstream head above crest and L_{crest} is the crest length (L_{crest} = 0.6 m). The results were quantitatively comparable to the findings of Pfister (2009). There were however some distinctive difference across the range of flow conditions, the worst deflecting jet conditions being observed for 0.18 < H_1/L_{crest} < 0.27. For these conditions, deflecting jets took off at step edges 1 and 4, while large air cavities formed between step edges 1-3 and between step edges 4-6 respectively.

Further a series of tests were performed systematically with a monotonically increasing discharge, followed by a monotonically decreasing flow rate. The results showed some marked hysteresis. The above quantitative observations were obtained with increasing discharges.

Figure 5. Jet deflections at the downstream end of a sharp edged weir (step edge 1) and at step edge 4 - Red arrows point to the jet detachment - The first nappe re-attached at step edge 3, and the second jet re-attached at step edge 8 - Flow conditions: q = 0.075 m^2/s, h = 0.1 m, L_{crest} = 0.6 m, H_1/L_{crest} = 0.21

3.3 Stepped chute

Three flow regimes were observed on the stepped chute. For small discharges ($d_c/h < 0.4$), a nappe flow regime occurred. The rounded nose on step edge 1 guided the overflow along the step rise. A series of free-falling nappes were observed past step edge 2. At very low discharges, the flow appeared highly irregular in the transverse flow direction and some unstable flapping was observed. For an increase in discharge above $d_c/h > 0.15$, the small nappes were replaced by a clear supercritical jet downstream of step edge 2 and an aerated jet above step edge 5.

For an intermediate range of discharges ($0.4 < d_c/h < 0.9$) a transition flow regime was identified. The overflow was characterised by strong hydrodynamic instabilities and chaotic splashing. For $d_c/h < 0.6$, a large coherent water jet deflected off step edge 2 and stagnated on step 5. All step cavities downstream of step edge 5 were partially filled, with alternating cavity sizes from small to medium. The upstream jet disappeared once d_c/h exceeded 0.6 and all step cavities became partially filled.

For $d_c/h > 0.9$, a skimming flow was observed. The overflow skimmed over the pseudo-bottom formed by step edges. The streamlines were approximately parallel and the free-surface exhibited a wavy profile approximately in phase with the steps. At the upstream end the flow was smooth and glassy. Downstream of the inception of aeration some complex air-water interactions were observed. The flow in step cavities exhibited a stable recirculation motion characterised by self-sustaining vortices. A close examination of the cavity vortical structures showed irregular ejection of fluid from the cavity into the mainstream flow next to the upper vertical step face, and replacement of cavity fluid next to the step edge, in manner similar to the observations of Djenidi et al. (1999) and Chanson and Toombes (2002a). The observation indicated strong mainstream-cavity flow interactions.

4. Flow properties

4.1 Broad crested weir

The free surface profiles measured above the broad-crested weir implied an accelerating flow along the crest and some non-hydrostatic pressure gradients. Figure 6 presents the dimensionless water depth $d \times \Lambda/H_1$ as a function of the dimensionless coefficient $\beta \times C_D^2 \times \Lambda^2$ for $0.17 < x/L_{crest} < 0.83$, where d is the flow depth, H_1 is the upstream head, x is the streamwise distance from the upstream vertical wall, y is the distance normal to the crest, L_{crest} is the crest length, β is the Boussinesq coefficient (or momentum correction coefficient), C_D is the discharge coefficient, and Λ is the dimensionless pressure coefficient. In Figure 6, the red and black lines represent two of the four physical solutions to an energy equation proposed for a smooth, frictionless flow with non-hydrostatic pressure distributions (Chanson 2006). A good agreement was found between the data and theoretical predictions. This suggests that critical flow conditions occurred along the broad crest despite some water surface curvature and energy loss in the boundary layer. Similar findings were reported for a rounded broad-crested weir with a length of 1.01 m (Felder and Chanson 2012).

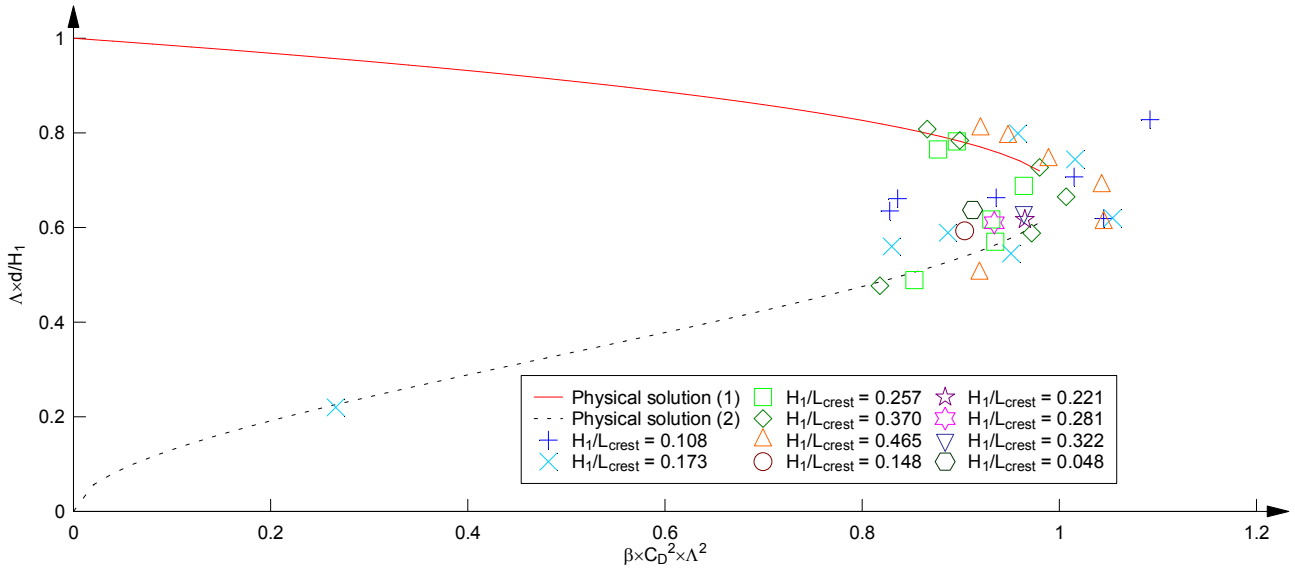

Figure 5. Dimensionless flow depth as a function of pressure, momentum and discharge coefficients

Measured pressure and velocity distributions above the broad-crested weir are presented in Figure 6 in dimensionless terms for H_1/L_{crest} = 0.37. The results highlighted some variation in pressure and velocity profiles along the weir crest. The pressure gradient (Figure 6A) was typically hydrostatic in the middle of the crest, and non-hydrostatic at the upstream and downstream ends of the weir crest resulting from the free-surface curvature. The vertical velocities derived from the free-surface slope were in the order of 0.2 – 0.3 m/s. The velocity distributions revealed an accelerating flow along the crest with a developing boundary layer underneath.

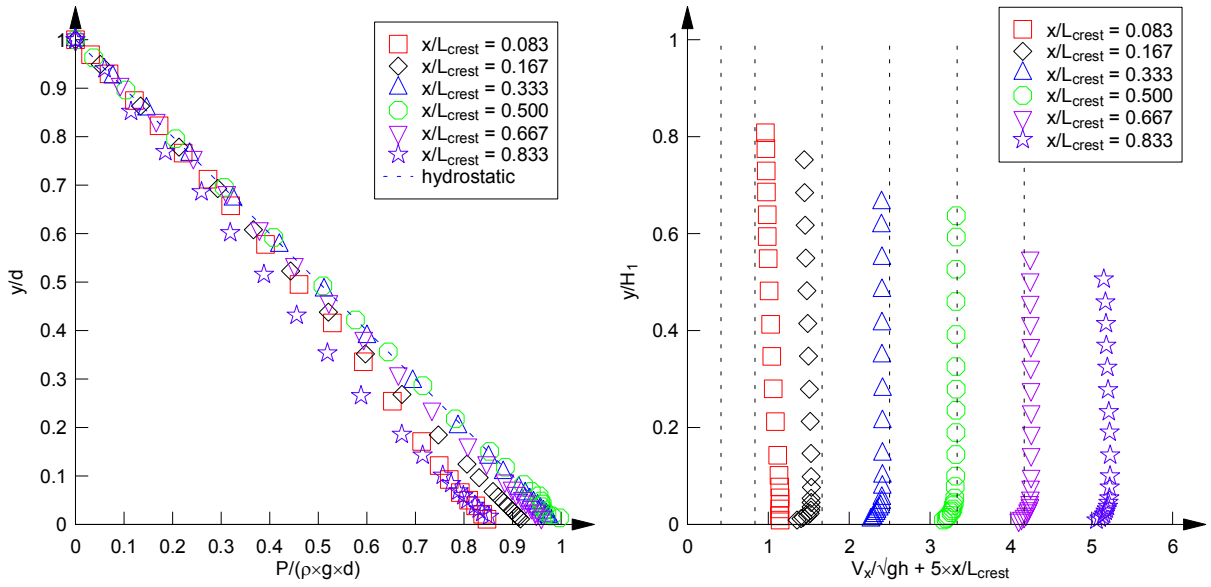

(A) Dimensionless pressure distributions (B) Dimensionless velocity distributions

Figure 6. Dimensionless pressure and velocity distributions above a broad crested weir – H_1/L_{crest} = 0.370

The redistributions of velocity and pressure at the upstream end of the crest were associated with flow acceleration. Above the horizontal crest, the no-slip condition at the invert induced a boundary layer growth. Earlier measurements suggested that the virtual origin of the boundary layer could be a short distance upstream of the crest (Harrison 1967). The boundary layer growth was estimated from velocity data and presented in Figure 7. In Figure 7, δ is the boundary layer thickness defined as the depth where V equals 99% of the free stream velocity, and μ is the dynamic viscosity of water. The present data showed a boundary layer growth rate of approximately $\delta \sim x^{0.56}$, closer to a laminar ($\delta \sim x^{0.5}$) rather than a turbulent ($\delta \sim x^{0.8}$) boundary layer (Schlichting 1960, Chanson 2009). This rate is similar to that reported by Gonzalez and Chanson (2007). The maximum length Reynolds number achieved in the current investigation was 6.1×10^5, approximately twice compared to a transition at 3×10^5 (Harrison 1967). The boundary layer in the present study

is therefore laminar over approximately the first half of the weir crest and partly turbulent thereon. For large discharges the favourable pressure gradient (dP/dx > 0) implied by the downward-sloping free-surface would also need to be taken into account, and thus may explain some of the discrepancies with boundary layer theories developed based on a zero pressure gradient assumption. Note the decrease in boundary layer thickness towards the downstream end of the crest. This may be associated with the velocity redistribution influenced by the downstream drop, and was also reported in a previous study (Felder and Chanson 2012).

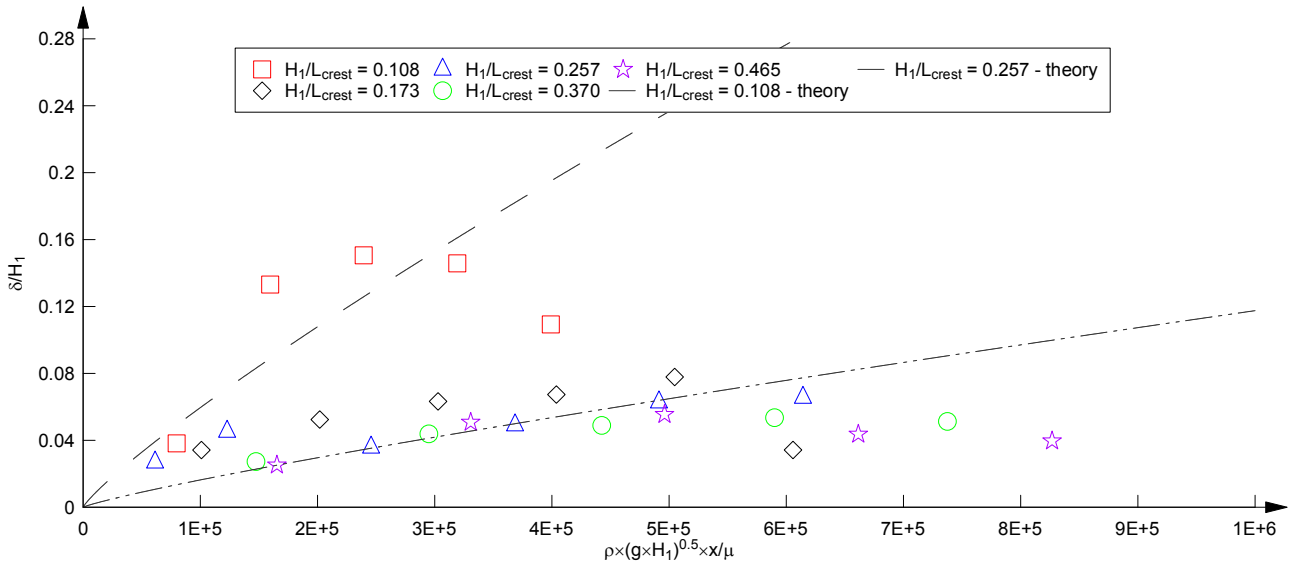

Figure 7. Boundary layer growth above broad-crested weir

The velocity data at the middle of the crest (x/L_{crest} = 0.5) were integrated to obtain the discharge. Figure 8 summarises the discharge coefficients obtained as a function of dimensionless upstream head. A linear increase in C_D was observed for an increasing discharge, similar to most comparison data presented (Bazin 1896, Felder and Chanson 2012). The discharge coefficient was less than unity for small discharges because of energy loss in the laminar boundary layer. For large discharges, C_D slightly exceeded 1, because the crest length was too short compared to the flow depth and the streamlines above the crest could no longer be assumed parallel. The best fit (Figure 8) of the present data matched all comparison data reasonably well, except that of Gonzalez and Chanson (2007). The discrepancy stems from generation of corner eddies next to the sidewalls upstream of the weir, which caused some blockage effect and flow instabilities (Gonzalez and Chanson 2007).

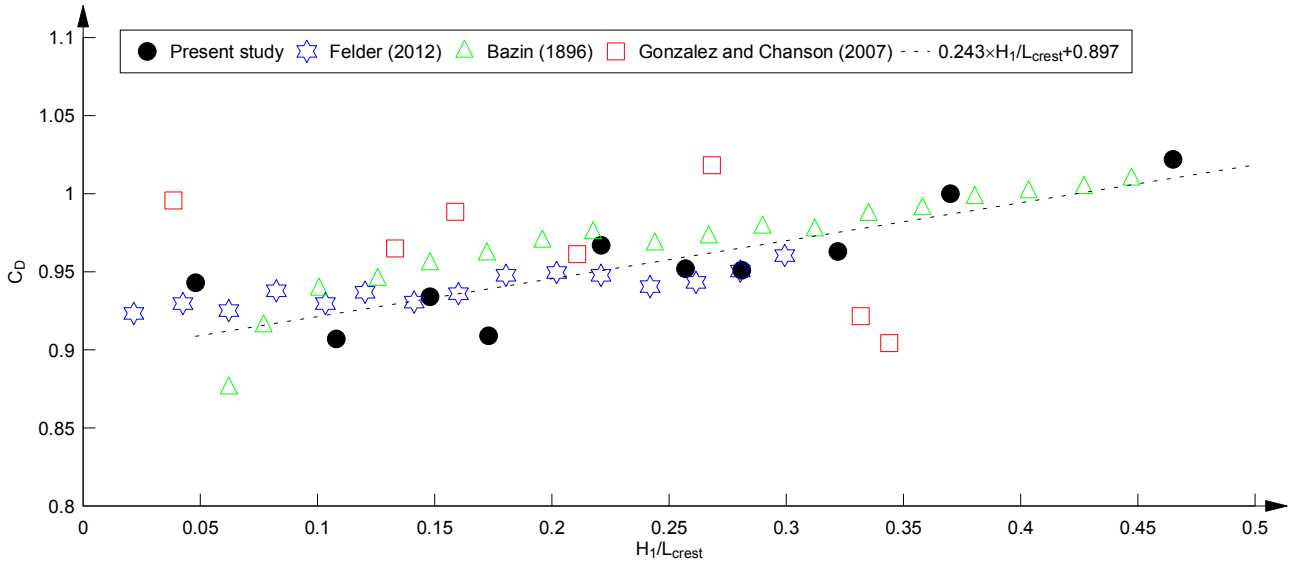

Figure 8. Discharge coefficient as a function of dimensionless upstream head

4.2 Stepped chute

Downstream of the broad-crested weir, the turbulence interactions next to the surface caused a large amount of air to be entrained. The two-phase flow properties were measured using a dual-tip phase detection probe and typical results are presented in Figure 9. In Figure 9, C is the void fraction, Y_{90} is the depth for C = 0.9, and V_c is the critical velocity. The void fraction profiles (Figure 9A) above all step edges presented an inverted S-shape, typical for flat steps (Chanson and Toombes 2002b, Gonzalez and Chanson 2008, Felder 2013). The results followed closely a theoretical solution (Chanson and Toombes 2002b). All void fraction profiles were self-similar except immediately downstream of the inception point (step edge 7), where the flow was rapidly varied. The bubble count rate (Figure 9B) is defined as half the number of air-water interfaces detected by the probe sensor per second. The data showed a distinct bell shape, with a maximum in the middle of the shear layer ($y/d_c \approx 0.4$), with a corresponding void fraction of approximately 0.5.

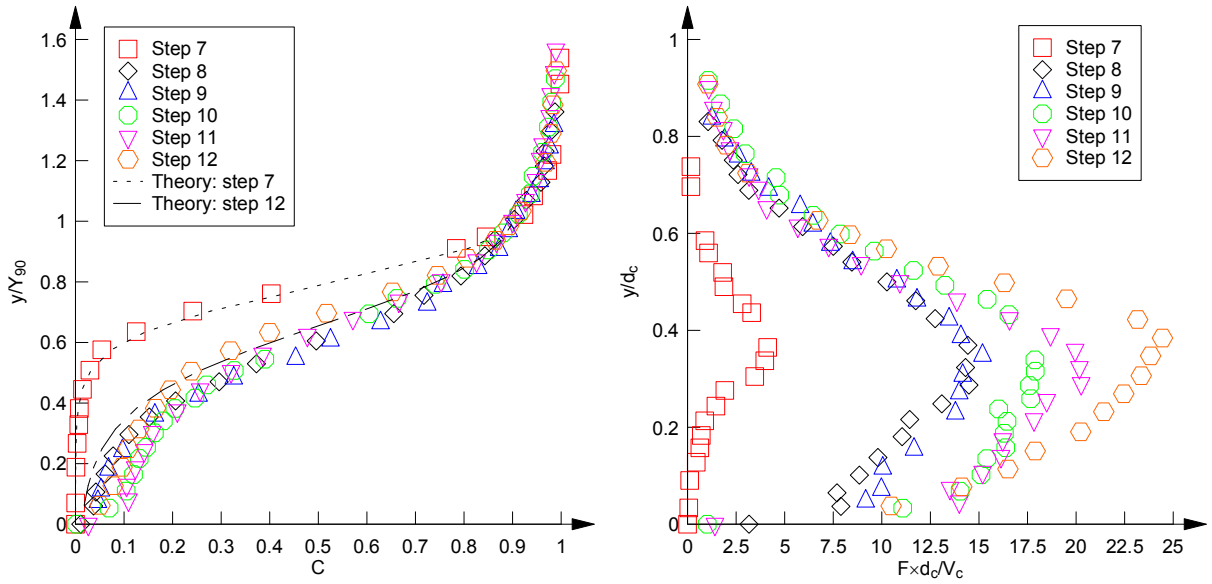

(A) Void fraction distributions (B) Bubble count rate distributions

Figure 9. Two-phase flow properties in a skimming flow above the stepped chute – $d_c/h = 1.3$

The interfacial velocity (V) and turbulence intensity (Tu) profiles were calculated based upon a cross-correlation technique between the probe signals, and typical results are presented in Figure 10. In Figure 10, V_{90} is the velocity at Y_{90}. The velocity profiles (Figure 10A) were self-similar, and followed closely a 1/10 power law. The shape highlighted a developing shear layer in the wake of the step edge. The turbulence intensities revealed a maximum in the mid-water column, close to the locations of maximum bubble count rates. The largest turbulence levels were recorded at the first step edge downstream of the inception point (step edge 7), which may be associated with some flow instabilities in the surrounding flow region.

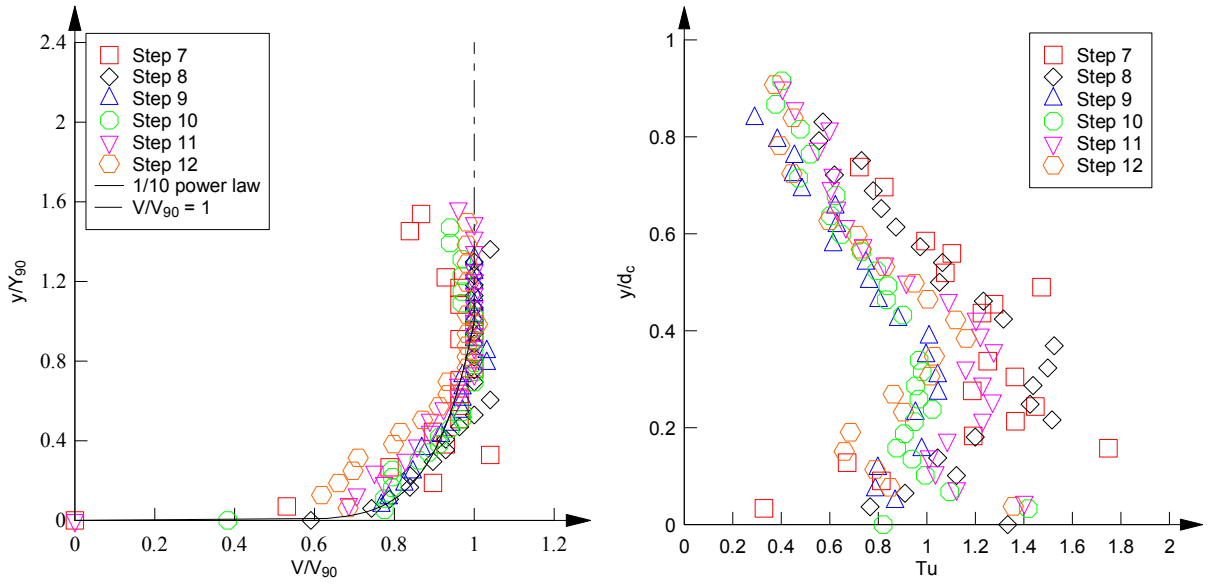

(A) Interfacial velocity distributions (B) Turbulence intensity distributions

Figure 10. Interfacial velocity and turbulence intensity distributions above the stepped chute – d_c/h = 1.3

On a stepped chute, the steps not only contribute to intense-air-water mixing but also to energy dissipation. Figure 10 illustrates the energy dissipation performances of the present configuration, where N is the step edge number, ΔE is the total head loss, E_t is the total head (taking the stilling basin as the datum), h =0.1 m is the step height, and H_{res} is the residual energy calculated based upon the air-water flow measurements, assuming an energy correction coefficient α = 1. The results demonstrated substantial energy dissipation along the stepped chute, with up to 60% of total energy dissipated before reaching the stilling basin (Figure 11A). The results were close for all discharges. Figure 11B plots the dimensionless residual head as a function of discharge. The downstream residual head (step edge 12) decreased with increasing discharge, showing a close agreement with earlier studies (Felder and Chanson 2011,2014). The finding implied that the chute slope might be a factor that determines energy dissipation performance. Note that the largest Reynolds number investigated was 7.7×10^5.

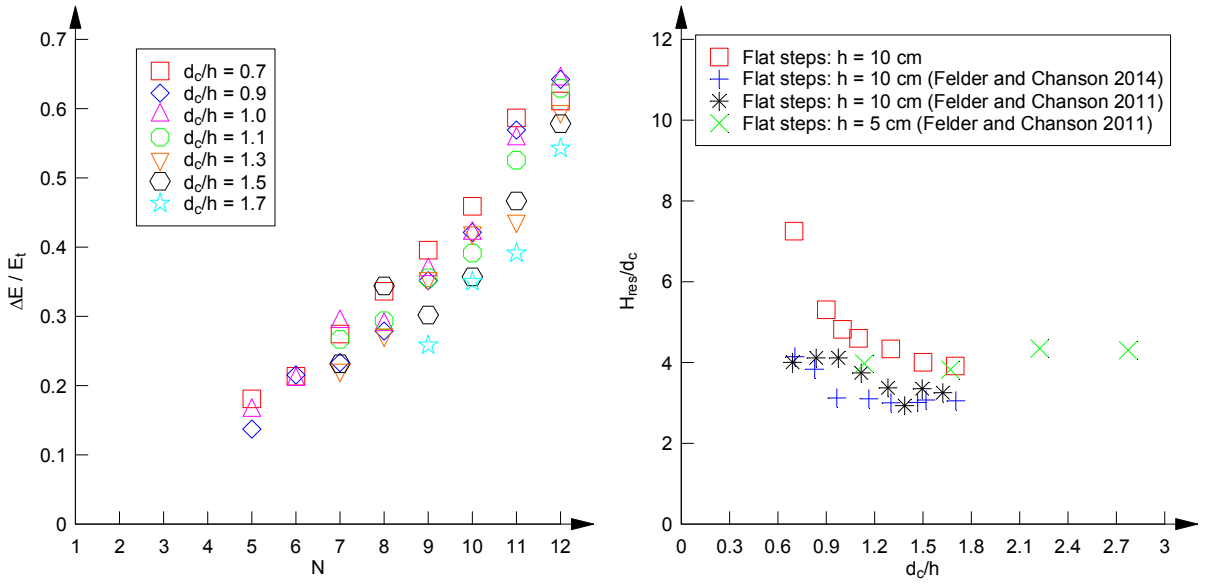

(A) Total head loss along stepped chute (Present study) (B) Residual head above the last step edge

Figure 11. Energy dissipation in the aerated flow region on a stepped chute

It is common to express the flow resistance using the Darcy-Weisbach friction factor f_e (Rajaratnam 1990, Chanson 2001,2006b), despite some views that this might be inappropriate for step-induced form losses (Chanson et al. 2002). Herein the friction factors were derived from measured friction slope (derived from air-water measurements) and water discharge. The results are presented in Figure 12. In Figure 12, the horizontal axis is the cavity height normalised by the hydraulic diameter D_H. The data yielded friction factors between 0.1 and 0.3, slightly below findings on a flatter slope (Felder and Chanson 2011, 2014).

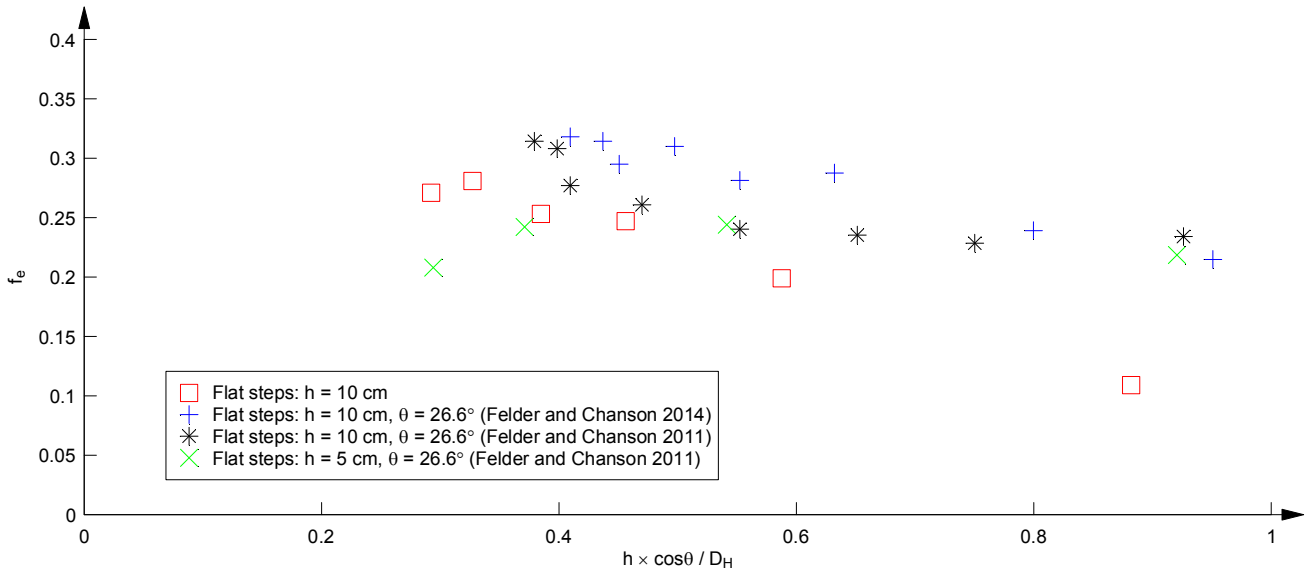

Figure 12. Darcy-Weisbach friction factor in the air-water flow on the stepped chute

5. Conclusion

Detailed measurements were undertaken above a large-size stepped spillway physical model. The pressure and velocity distributions above the broad-crested weir were measured with a Prandtl-Pitot tube. The two-phase flow properties in the stepped chute were examined with a dual-tip phase detection probe.

The flow above the broad-crested weir was quiescent and smooth. The installation of a small rounding downstream of the weir was proven as a simple mean to control the deflecting jet. The flow was critical along the crest and rapidly varied at each end. The pressure distributions were influenced by the free-surface curvature. The velocity profiles revealed an accelerating flow above a developing boundary layer. The discharge coefficient increased linearly with increasing discharge, subject to energy loss and crest length.

Intense air-water interactions were observed down the stepped chute. Downstream of the inception point of free-surface aeration, the flow was highly aerated and the void fraction profiles followed an inverted s-shape distribution. The bubble count rate profiles showed a maximum in the mid-water column. The velocity profiles were self-similar and modelled by a 1/10 power law. Turbulence intensities were maximum in the middle of the shear layer. Energy dissipation rates up to 60% were achieved down the 12 steps. The estimated friction factors ranged between 0.1 and 0.3, and were smaller than those on a stepped spillway with a flatter slope.

ACKNOWLEDGMENTS

The authors acknowledge the technical assistance of Jason Van de Gevel and Stewart Matthews. The financial support of Australian Research Council (Grant DP120100481) is acknowledged.

REFERENCES

Bazin, H. (1896). Expériences nouvelles sur l'ecoulement par déversoir [recent experiments on the flow of water over weirs]. Mémoires et Documents, Annales des Ponts et Chaussées, Paris, France, Sér. 7,Vol. 12, 2nd Sem., 645–731 Plates (in French) (referenced in Felder and Chanson 2012).

Chanson, H. (1995). History of Stepped Channels and Spillways : a Rediscovery of the 'Wheel'. Can Jl of Civ. Eng., Vol. 22, No. 2, April, pp. 247-259.

Chanson, H. (2001). The Hydraulics of Stepped Chutes and Spillways. Balkema, Lisse, The Netherlands, 418 pages.

Chanson, H. (2006). Minimum Specific Energy and Critical Flow Conditions in Open Channels. Journal of Irrigation and Drainage Engineering., ASCE, Vol. 132, No. 5, pp. 498-502 (doi:10.1061/(ASCE)0733-9437(2006)132:5(498))

Chanson, H. (2006b). Hydraulics of Skimming Flows on Stepped Chutes: the Effects of Inflow Conditions? Journal of Hydraulic Research, IAHR, Vol. 44, No. 1, pp. 51-60.
Chanson, H. (2009). Applied Hydrodynamics: An Introduction to Ideal and Real Fluid Flows. CRC Press, Taylor & Francis Group, Leiden, The Netherlands, 478 pages.
Chanson, H., and Toombes, L. (2002a). Air-Water Flows down Stepped chutes. Turbulence and Flow Structure Observations. International Journal of Multiphase Flow, Vol. 28, No. 11, pp. 1737-1761.
Chanson, H., and Toombes, L. (2002b). Energy Dissipation and Air Entrainment in Stepped Storm Waterway. Experimental Study. Journal of Irrigation and Drainage Engineering, ASCE, Vol. 128, No. 5, pp. 305-315.
Chanson, H., Yasuda, Y., and Ohtsu, I. (2002). Flow Resistance in Skimming Flows and its Modelling. Canadian Journal of Civil Engineering, Vol. 29, No. 6, pp. 809-819.
Djenidi, L., Elavasaran, R., and Antonia, R.A. (1999). The Turbulent Boundary Layer over Transverse Square Cavities. Jl Fluid Mech., Vol. 395, pp. 271-294.
Felder, S. (2013). Air-Water Flow Properties on Stepped Spillways for Embankment Dams. Aeration, Energy Dissipation and Turbulence on Uniform, Non-Uniform and Pooled Stepped Chutes. Ph.D. thesis, School of Civil Engineering, The University of Queensland, Brisbane, Australia.
Felder, S., and Chanson, H. (2011). Air-Water Flow Properties in Step Cavity down a Stepped Chute. International Journal of Multiphase Flow, Vol. 37, No. 7, pp. 732–745.
Felder, S., and Chanson, H. (2012). Free-surface Profiles, Velocity and Pressure Distributions on a Broad-Crested Weir. a Physical study. Journal of Irrigation and Drainage Engineering, ASCE, Vol. 138, No. 12, pp. 1068–1074.
Felder, S., and Chanson, H. (2014). Effects of Step Pool Porosity upon Flow Aeration and Energy Dissipation on Pooled Stepped Spillways. Journal of Hydraulic Engineering, ASCE, Vol. 140, No. 4, Paper 04014002, 11 pages.
Felder, S., and Chanson, H. (2015). Phase-Detection Probe Measurements in High-Velocity Free-Surface Flows including a Discussion of Key Sampling Parameters. Experimental Thermal and Fluid Science, Vol. 61, pp. 66-78.
Gonzalez, C.A., and Chanson, H. (2007). Experimental Measurements of Velocity and Pressure Distribution on a Large Broad-Crested Weir. Flow Measurement and Instrumentation, Vol. 18, pp 107-113.
Gonzalez, C.A., and Chanson, H. (2008). Turbulence Manipulation in Embankment Stepped Chute Flows: an Experimental Study. European Journal of Mechanics B/Fluids, Vol. 27, No. 4, pp. 388-408.
Harrison A.J.M. (1967). The streamlined broad-crested weir. Proc Inst Civil Eng 1967;38.657–678; Discussion 1969;42.575–99.
Knauss, J. (1995). Σ ΤΟ ΠΗΔΗΜΑ, der Altweibersprung. Die Rätselhafte Alte Talsperre in der Glosses-Schlucht bei Alyzeia in Akarnanien. Archäologischer Anzeiger, Heft 5, pp. 138-162 (in German).
Novak, P., Moffat, A.I.B., Nalluri, C., and Narayanan, R. (2001). Hydraulic Structures. Spon Press, London, UK, 3rd edition, 666 pages.
Pfister, M. (2009). Effect of Control Section on Stepped Spillway flow. Proc. 33rd IAHR Biennial Congress, IAHR-ASCE-EWRI, Vancouver, Canada, 9-14 Aug., 8 pages.
Schlichting, H. 1960. Boundary layer theory, 4th Ed., McGraw-Hill, New York.
Schuyler, J. D., 1909. Reservoirs for Irrigation, Water-Power and Domestic Water Supply, 2nd edn. New York: Wiley.
Toombes, L. (2002). Experimental Study of Air-Water Flow Properties on Low-Gradient Stepped Cascades. Ph.D. Thesis, Dept. of Civil Engineering, University of Queensland, Australia.
USBR (1965). Design of Small Dams. Bureau of Reclamation, US Department of the Interior, Denver CO, USA, 3rd edition.
Wegmann, E. (1907). The Design of the New Croton Dam. Transactions, ASCE, Vol. LXVIII, No. 1047, pp. 398-457.